Impact of the windbreak transition on flow structures of the high-speed railway and mitigation using oblique structure and circular curve structure transition

Zheng-Wei Chen

National Rail Transit Electrification and Automation Engineering Technology Research Center (Hong Kong Branch), Hung Hom, Kowloon, Hong Kong, China
Department of Civil and Environmental Engineering, The Hong Kong Polytechnic University, Hung Hom, Kowloon, Hong Kong, China

Guang-Zhi Zeng

National Rail Transit Electrification and Automation Engineering Technology Research Center (Hong Kong Branch), Hung Hom, Kowloon, Hong Kong, China
Department of Civil and Environmental Engineering, The Hong Kong Polytechnic University, Hung Hom, Kowloon, Hong Kong, China

Syeda Anam Hashmi

Birmingham Centre for Railway Research and Education, School of Civil Engineering, University of Birmingham B15 2TT, UK

Tang-Hong Liu

Key Laboratory of Traffic Safety on Track of Ministry of Education, School of Traffic & Transportation Engineering, Central South University, Changsha, 410083, China
Joint International Research Laboratory of Key Technology for Rail Traffic Safety, Changsha, 410083, China
National & Local Joint Engineering Research Center of Safety Technology for Rail Vehicle, Changsha, 410083, China

Lei Zhou

Department of Civil and Environmental Engineering, The Hong Kong University of Science and Technology, Clear Water Bay, Kowloon, Hong Kong, China

Jie Zhang

Key Laboratory of Traffic Safety on Track of Ministry of Education, School of Traffic & Transportation Engineering, Central South University, Changsha, 410083, China
Joint International Research Laboratory of Key Technology for Rail Traffic Safety, Changsha, 410083, China
National & Local Joint Engineering Research Center of Safety Technology for Rail Vehicle, Changsha, 410083, China

Hassan Hemida

Birmingham Centre for Railway Research and Education, School of Civil Engineering, University of Birmingham B15 2TT, UK

This work was supported by the National Natural Science Foundation of China (Grant No. 52202426), the National Key R&D Program of China (Grant No. 2020YFA0710903) and the Open Project of Key Laboratory of Traffic Safety on Track of Ministry of Education, Central South University (Grant No. 502401002).

Conflict of Interest: The authors declare that there is no conflict of interest.

Abstract

Purpose − This paper aims to investigate the variations in the flow fields induced by transition regions in the windbreak structures between the flat ground and the cutting along a railway, and to propose mitigation measures to improve the windproof ability of the windbreak.

Design/methodology/approach − The improved delayed detached-eddy simulation (IDDES) method was used to simulate the impact of the windbreak transition on flow structures of the high-speed railway under different wind angles, and also the accuracy of the numerical results were validated with those of the wind tunnel test.

Findings − The results showed that the original windbreak transition region resulted in a dimensionless peak wind velocity of 0.62 and 0.82 for railway line 1 at wind angles of 90° and 75°, respectively, and the corresponding values were 0.81 and 0.97 for railway line 2. The flow structure analysis revealed the reason for the mismatched height in the transition region, and the right-angle structures of the windbreaks resulted in ineffective protection and sudden changes in the wind speed and direction. Two mitigation measures—oblique structure (OS) and circular curve structure (CCS) transition walls—were developed to reduce the peak wind speed. The OS provided superior protection. The peak value of dimensionless wind velocity was all less than 0.2 for OS and CCS.

Originality/value − The flow field deterioration mechanism induced by the inappropriate form of a windbreak transition at different wind angles was examined, and effective mitigation and improvement measures were proposed and compared with the original transition.

Keywords Railway aerodynamics, Windbreak transition, CFD, Flow structures, Mitigation measures

Paper type Research paper

1. Introduction

Strong crosswinds on railways cause more concerns, as they threaten both the comfort and safety of the trains, with accidents every year (Diedrichs et al, 2007; Baker et al, 2009). The research on the aerodynamics (Krajnović et al, 2012; Cui et al, 2014; Liu et al, 2022) and dynamics (Shao et al, 2011; Li et al, 2013; Liu et al, 2019) of train subjected to crosswind has attracted wide attention and has been investigated all over the world. To identify the aerodynamic characteristics of different trains under crosswind, trains with different shapes have been studied by scholars, for instance, German ICE2 (Hemida and Krajnović, 2009), China high-speed train (Gao et al, 2021) and double unit train (Guo et al, 2019). Except for the shape of the train, the terrain types in the wind region are also the main influencing factor of train aerodynamics. Thus, there are many studies on the train passing through embankments (Diedrichs et al, 2007; Guo et al, 2020; Li et al, 2022), cutting (Ye and Li, 2013; Zhang et al, 2014), bridges (He et al, 2020) and tunnel (Chen et al, 2017) under crosswind. These studies provide a solid foundation for further studies on the safety of high-speed trains in wind region.

Under the knowledge that how crosswinds affect the safety of high-speed train, scholars have undertaken a series of studies to mitigate this wind effect, including optimising the train shape (Chen et al, 2018; Chen et al, 2019b), building the windproof facilities (Xiang et al, 2015; Gu et al, 2020; Niu et al, 2022), and developing wind

forecasting and warning systems (Tian, 2010; Tian, 2019). Among them, due to their economic advantages, ease of installation, reliability, and effectiveness, windbreak walls are a very promising solution. Therefore, different configurations can be studied to find the best models to implement, and such studies have been conducted by some researchers (Xiang et al, 2015; He et al, 2019; Gu et al, 2020). All the above studies were carried out under a certain terrain type, without considering the impact of the sudden change of wind from the geometric discontinuity and windproof facilities (windbreak transition).

In reality, there are geometric discontinuities around the railways, which will cause sudden flow changes and challenge the installation of various types of windbreak. Deng et al (2019) compared the aerodynamic loads and safety of a high-speed train as it passed through open-cut tunnel facilities, and it was found that at the entry points of an open-cut tunnel, the aerodynamic loads reached a peak for each carriage. Li et al (2019) researched the effects of the transition generated from a viaduct to a cutting on a 1:20 scale model train model under crosswinds and found that for a single train case, the side coefficients on the windward railway track were much higher than those on the leeward side. A windbreak breach may occur due to construction issues or an accident, and this effect on the train dynamic performance was studied by Sun et al (2019). It was found that shorter windbreak breaches resulted in higher wind speeds but lower wind loads compared to longer windbreak breaches.

Additionally, other factors can result in sudden wind speed changes, such as discontinuous windproof facilities. For example, the Lanzhou–Xinjiang passenger railway is a double line in China with a total length of 1776.9 km, and it is a railway that was built through an area with strong winds (Xu et al, 2019). Windbreaks were built along the railway, but part of the railway line passes through mountainous terrain. In addition, trains on the railway pass flat ground, embankments, and cuttings in some areas, as shown in Figure 1. Therefore, the windbreaks were built discontinuously. Full-scale tests were conducted and showed that when trains passed through transition regions of windbreaks, a yawing phenomenon occurred. The aerodynamic performance and dynamic index of a vehicle system showed sudden changes and became worse mainly in the position of the discontinuous transition region. This would have an effect on both passenger comfort and operational safety. Focusing on this issue, the effect of wind speed variations on the dynamics of a high-speed train was studied by Liu et al (2019), who considered the wind speed ramp time, peak wind speeds at different mean wind speeds, and peak wind speed duration. The ideal wind speed curve was produced, while the effects of different factors on the safety of the train were studied. Real terrain was also considered, and a computational fluid dynamics method was used in combination with different dynamic models. Liu et al (2018) and Chen et al (2019a) investigated the aerodynamic performances and the dynamic response when a train passed through such transition regions under crosswinds.

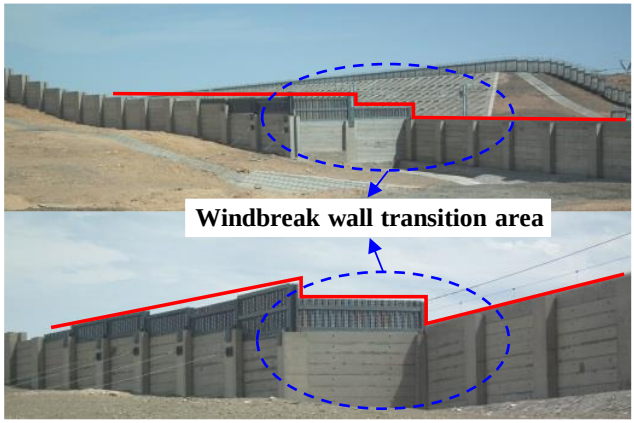

Figure 1. Windbreak transitions in the railway.

In fact, the most direct method to provide useful information for the safety of train operation is to study the variation of flow field around the train and its aerodynamic force as the train passes through the transition section under crosswinds, as our previous work reported (Chen et al, 2022). It is worth mentioning that the previous work on transition regions in windbreaks has provided various insights into this critical issue. However, these studies mainly focused on the train while ignoring how the flow field deteriorates around the transition regions, which does not help much in the design and optimization of the windproof facilities. It is also important to understand the impact of transition regions on the flow field, and dive into the deterioration mechanism of the flow field in the transition regions, which is highly beneficial to the design and optimization of windproof facilities. Therefore, this work aims to study the changes in the flow fields induced by transition regions in the windbreak structures between the flat ground and the cutting without a train. Furthermore, based on the flow field analysis of the original windbreak transition and motivated by the studies on the boundary transition section in the truncated terrain model (Kondo et al, 2002; Hu et al, 2015; Huang et al, 2018), the improvement and mitigation measures (OS and CCS) are proposed and compared with the wind speed distribution and flow structures of the original transition.

The rest of this paper is organised as follows. Section 2 details the numerical simulations, while Section 3 provides analysis of the original windbreak transition, including the wind speed changes and flow field structure analysis. Section 4 proposes mitigation measures to allow the wind speed and flow field to change smoothly in the transition region. The main conclusions of this work are listed in Section 5.

2. Numerical simulation details

2.1 Model description

To reflect a case that is closer to practice, Figure 2 presents the windbreak transition models from the flat ground to the cutting. The length of the flat ground and cutting were both 200 m. The length of the windbreak transition region was 15 m, and the width was 10 m. The windward side (WWS) boundary was 60 m from the centre of the double railway lines, and the leeward side (LWS) boundary was 80 m from the same position. Figure 2(b) shows the cross-sectional drawing of the railway lines. It was a double railway line, and railway line-1 (RL-1) was close to the windbreak. The lateral distance between the two lines was 5 m, and the centre of RL-1 was 5.7 m from the windbreak.

The windbreak was 4 m in height and 0.2 m in width. Additionally, the highest wind speeds 35 m/s, and wind angles of 90°, 75°, and 105° were studied in the present work. Note that the full-scale size is shown to provide an intuitive understanding, and a 1/25 scaled-down model was used for this study. The general height is denoted as H, and a value of 3.7 m for a high-speed train in China was selected to make the distance and lengths dimensionless. The wind speed was expressed by the dimensionless coefficient u_i, $u_i = V_i / U$, where V is the wind speed above the railway, U is the upstream flow speed, and i represents the x, y, and z directions.

2.2 Numerical method and computational domain

The improved delayed-detached eddy simulation (IDDES) method based on the SST (shear stress transport) $k-\omega$ turbulence model was used in this paper. This hybrid numerical method was developed by Shur et al (2008) and was based on the Reynolds-averaged Navier–Stokes (RANS) and large eddy simulation (LES). This method was used in previous studies and demonstrated reliable performances in terms of experimental validation and flow structure analysis (Flynn et al, 2014; Huang et al, 2016; Wang et al, 2019). It was well known that for the traditional DES method, the RANS model is used for thin boundaries and the LES model is used for regions of massive separation (Wang et al, 2017). The resolution of the grid needs to be carefully considered when taking into account thick boundary layers with shallow separation regions. The grid spacing parallel to the wall was less than the thickness of the boundary layer or the increasing thickness of the boundary layer for a refined grid. In both cases, the DES length scale could be determined by the LES component, but it exhibited incorrect behaviour, as the resolution was not fine enough to support the LES model (Tahani et al, 2017). This is known as modelled-stress depletion (MSD), and it leads to premature separation, known as grid-induced separation. To solve this problem, a new subgrid length-scale was defined in the delayed detached eddy simulation (DDES) approach developed by Spalart et al (2006). Furthermore, in the present IDDES method, the wall-model LES (WMLES) method was used based on the DDES method to negate the limitation of the Reynolds number in the near-wall regions (Liu et al, 2017). Therefore, the IDDES included two components: DDES and WMLES models, as well as a set of empirical functions to obtain good performances from these components and their coupling.

In this paper, the governing equations were solved using the finite volume method (FVM) by the Fluent solver. The pressure–velocity coupling scheme was the Semi-Implicit Method for Pressure Linked Equations-Consistent (SIMPLEC) algorithm developed by (Van Doormaal and Raithby, 1984). The convective fluxes in the momentum equations were discretised using bounded central differencing, whereas the turbulent kintic energy and turbulent dissipation rate used the second-order upwind scheme. The time integration was conducted using a second-order backward implicit scheme. The time step was maintained at 1×10^{-4} s, and the maximum number of iterations was set to 30 for each time step. The Courant–Friedrichs–Lewy (CFL) numbers for the model were less than 1 in more than 90% of the computational cells during the entire simulation.

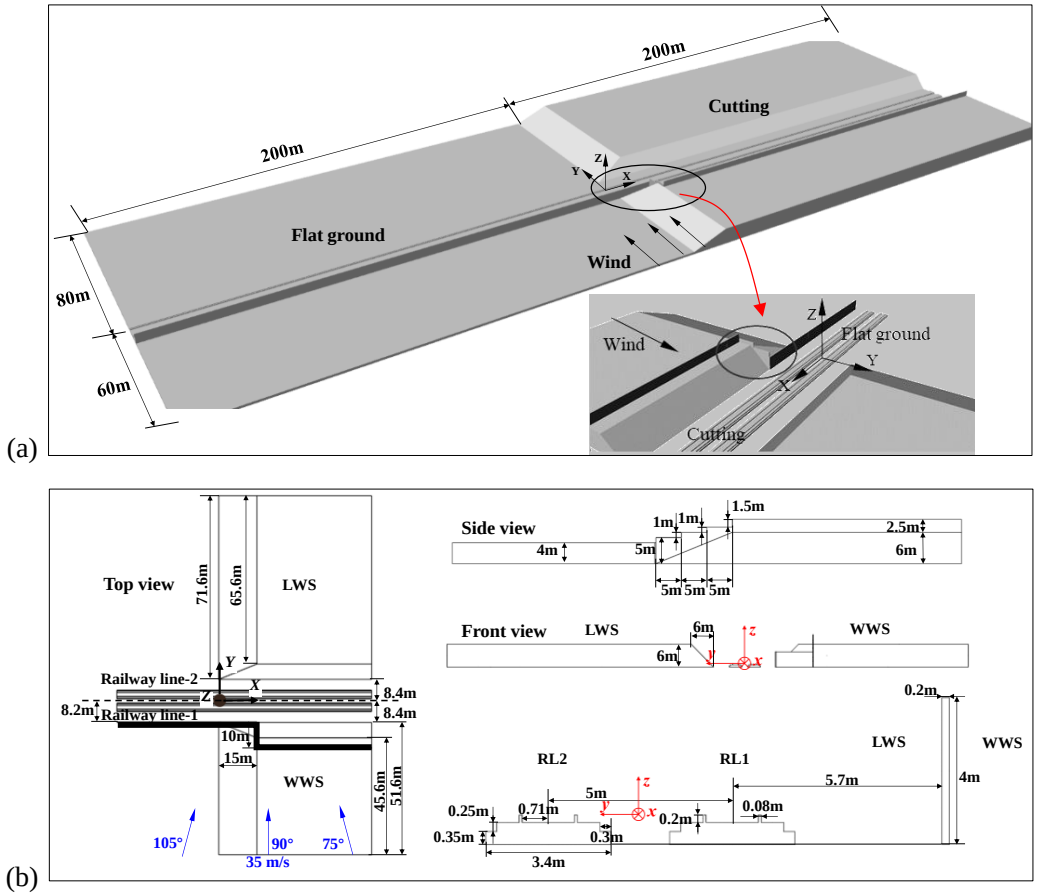

Figure 2. Computational models: (a) the 3D view of model and (b) the detail size of model.

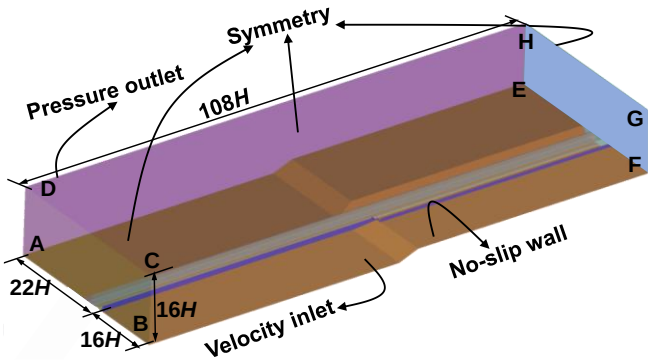

Figure 3. The computational domain and boundary conditions at wind angle 90°.

Figure 3 shows the computational domain and boundary conditions in the case of a wind angle of 90°. The face BFGC was a velocity inlet, the face AEHD was zero-pressure outlet. The ground, windbreak, and railway lines were no-slip walls. The other faces, ABCD, DCGH, and EFGH, were symmetry boundaries. For the case of a wind angle of 75°, faces EFGH and BFGC were set as velocity inlets, and faces ABCD and AEHD were set as zero-pressure outlets. The other boundary conditions remained the same. For the case with a wind angle of 105°, the faces ABCD and BFGC were set as velocity inlets, and the faces EFGH and AEHD were set as zero-pressure outlets. The other boundary conditions remained the same.

2.3 Mesh strategy

Figure 4 shows different views of the computational mesh and an enlarged view of the windbreak. The computational mesh in the present work was an unstructured hexahedral grid and was generated using SnappyHexMesh in OpenFOAM. In the windbreak transition regions, the flow separation takes place on the top of the windbreak due to the obstruction of the windbreak, causing the large separated flow region behind the windbreak, which is the main factor affecting the safety of trains operation. To resolve this strong separation region accurately, the mesh around the windbreak transition region will be very fine, while the mesh far away from this region will be progressively coarser to reduce the cells. Comparing to the separation region locating at the railway, the effect of wall-bounded flow on the train is not very obvious and will be modelled by the wall function in this study. There were 10 prism layers around the model and the minimum size around the model was 0.07 mm, resulting in a y^+ value was less than 10 on the model surface. According to the ANSYS Fluent Theory Guide (ANSYS, 2013), the ω-equation can be integrated through the viscous sublayer by using a y^+-insensitive wall treatment, which blends the viscous sublayer formulation and the logarithmic layer formulation based on y^+. This formulation was the default option for all ω-equation-based models, which was used to find the shear stress at the first cell close to the wall to ensure that the calculation was feasible. Additionally, to test mesh independence, three meshes were compared in this work: coarse, medium, and fine meshes, with corresponding mesh numbers of 10, 28, and 46 million, respectively. Along the railway centre at a wind angle of 90°, the dimensionless wind speeds, u_y, of the different meshes at z/H = 0.81 are shown in Figure 5. The error between the coarse mesh and other meshes was evident. However, the differences between the medium and fine meshes were very small. Therefore, a finer mesh was not required.

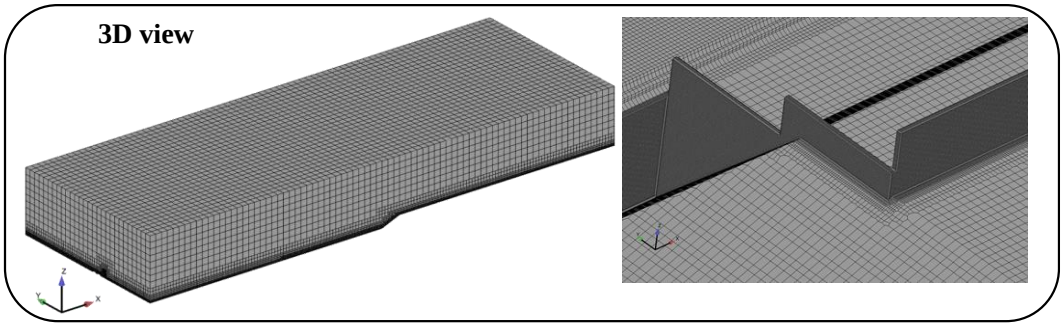

(a)

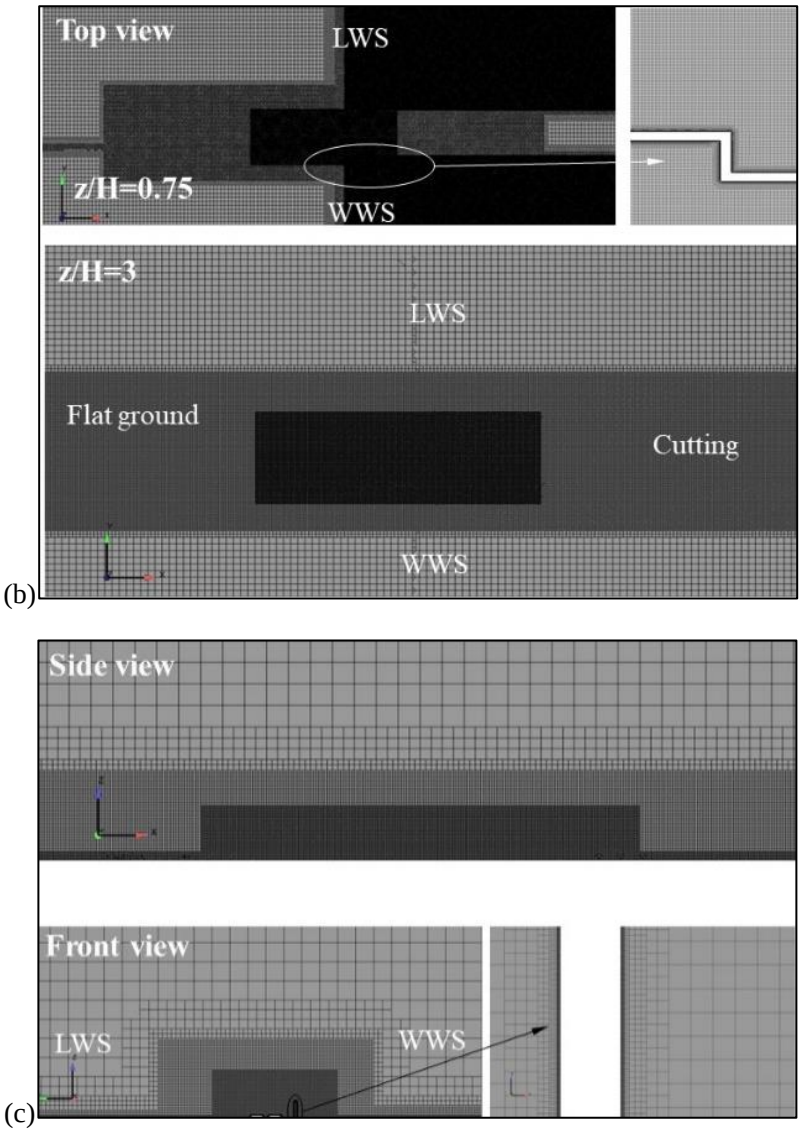

Figure 4. The computational mesh.

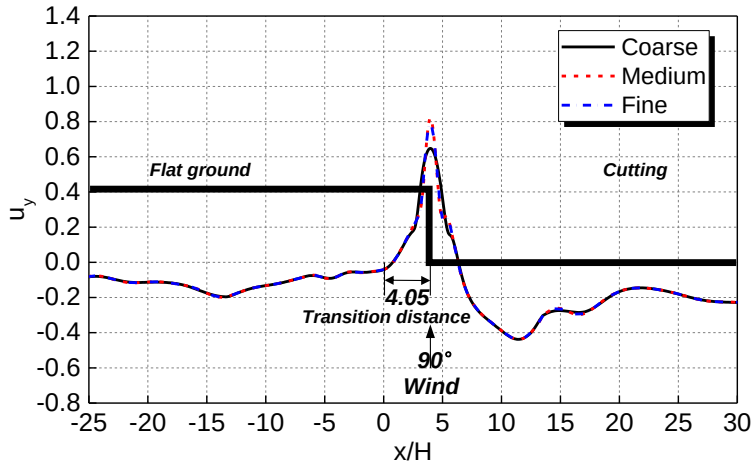

Figure 5. Result comparison between different meshes ("4.05" represents the transition distance x/H = 4.05).

2.4 Experimental validation

A wind tunnel test was conducted for the case consisting of a windbreak with a transition region in a flat ground scenario at the University of Birmingham, which was an open-circuit facility. The width and height of the wind

tunnel were 2 m each, and the length of the wind tunnel was 14 m. The centre position of the model was 10 m from the upstream inlet. The maximum freestream wind speed was approximately 10 m/s inside the wind tunnel. The test model is shown in Figure 6(a), along with a windbreak, a railway line, and a wooden plate as the ground scenario. To reduce the viscous effects of the ground, the model was installed at a height of 0.3 m above the floor of the wind tunnel. In addition, as shown in Figure 6(b), the wind speed was measured by a Cobra probe, which had a measurement frequency of 2 kHz (TFI, 2015). The test point of the upstream flow was 1.5 m from the front edge of the wooden plate, as shown in Figure 6(c). The upstream flow was measured at two heights, 0.5 m (top of the windbreak) and 0.8 m from the floor of the wind tunnel. The wind speed of the upstream flow was obtained using the average of these two heights, and the wind incidence angle was maintained at 90°. The models were 1:25 in scale. Above the centre of the tracks, the wind speed was tested at two heights, $h1$ = 0.252 m and $h2$ = 0.292 m. To measure the wind speed, 13 test points along the tracks were monitored at each height. During the tests, to reduce the random error, the wind speed at every test point was tested three times, and the average value of the three tests was calculated. With the same size and boundary conditions of the wind tunnel test, the simulation results from the medium mesh strategy are shown in Figure 7. The simulation results were in good arrangement with those of the wind tunnel test. It needs to note that the transition region studied in this paper actually is one part of the Lanzhou-Xinjiang railway in China, and the wind speed in this region is about 35m/s (Chen et al, 2021; Chen and Ni, 2022; Chen et al, 2022). Thus, to provide reference for the safety of train operation in this area, the freestream of baseline case was set as 35m/s in the simulation (Re = 8.87 × 10^6). On the other hand, limited by the experimental condition, the maximum freestream of 10m/s was used in the experiment (Re = 2.53 × 10^6). For the convenience of comparison, the freestream in the experimental validation is 10m/s. However, Both Reynolds numbers of the baseline and validation cases are greater than 10^6, locating on the self-similarity region, where the flow can be considered independent of the Reynolds number (Wu et al, 2013; Tschepe et al, 2021). Therefore, the methods validated in this session are also applicable for further study.

(a)

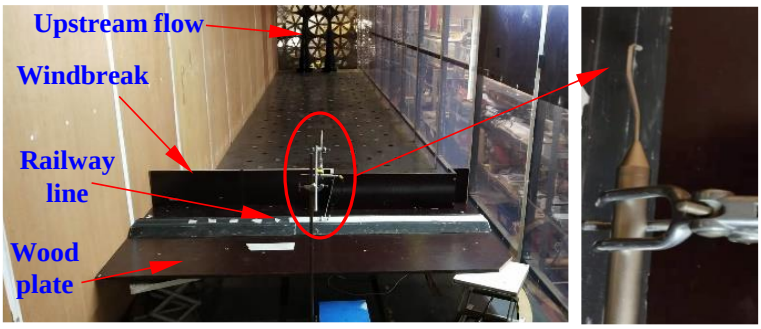

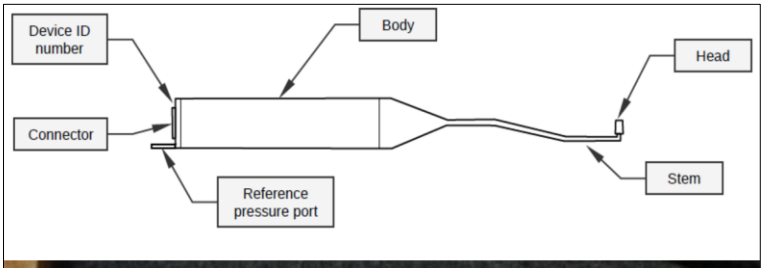

(b)

(c)

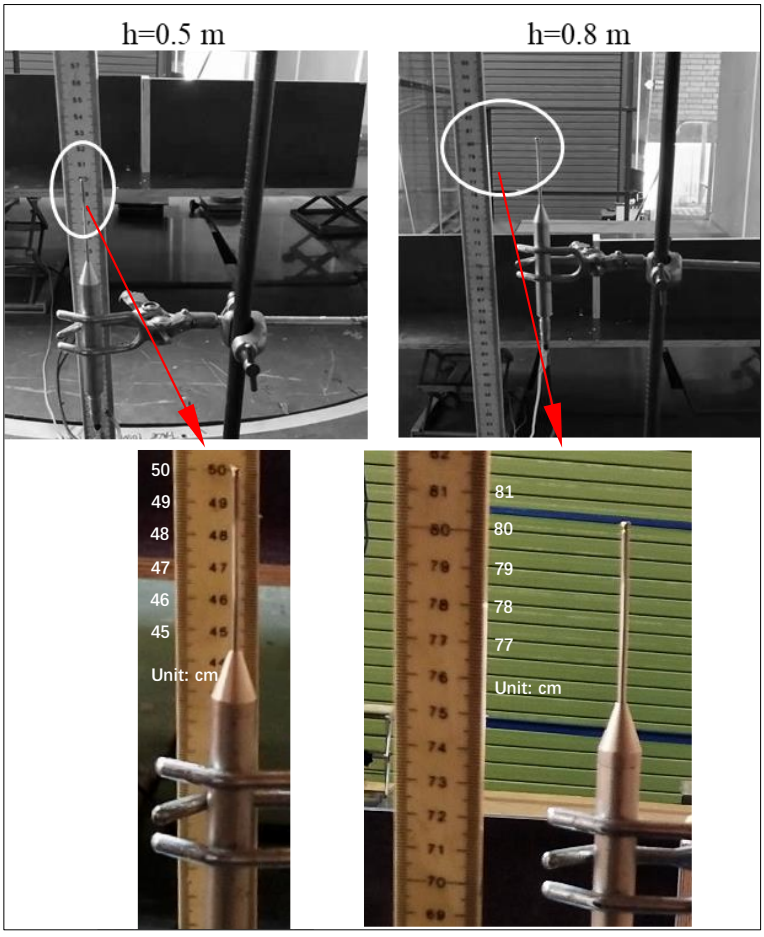

Figure 6. The test model: (a) the component of the test model, (b) the parameters of Cobra and (c) the test position of upstream flow.

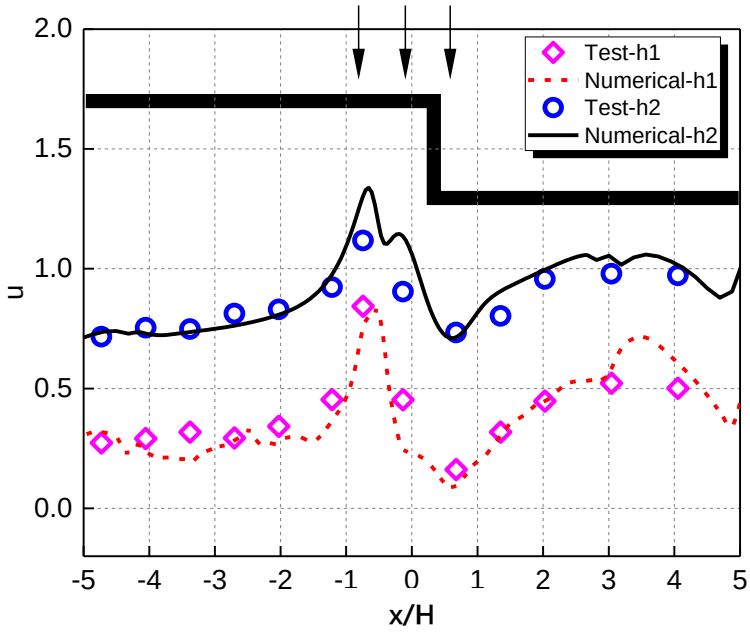

Figure 7. The comparison of results between the numerical simulation and wind tunnel test.

3. Analysis of original windbreak transition

3.1 Wind speed of original windbreak transition

As shown in Figure 8, the height z/H = 0.81 for RL-1 and RL-2 was chosen to analyse the change in the wind speeds of the railway. These points were located on the upper part of the train height range and could reflect the effect of wind on the train operation.

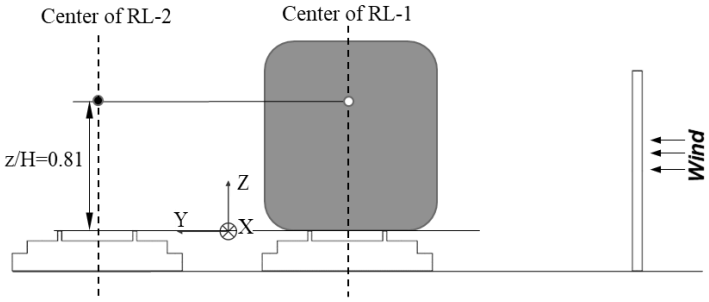

Figure 8. The analysis position of wind speed in the railway.

Figure 9 shows the wind speed along the railway for RL-1 and RL-2. With a wind angle of 90°, the peak value of u_y was 0.62 for RL-1 and 0.81 for RL-2. At a wind angle of 75°, the peak value was 0.82 for RL-1 and 0.97 for RL-2. At a wind angle 105°, the wind impact on the railway was weak, which was possibly due to the blocking effect of the connection slope between the flat ground and the cutting. Meanwhile, due to the effect of the windbreak transition with a wind angle of 90°, a negative value of −0.4 occurred after a peak positive value and returned to a smaller stable value. Overall, close to the flat ground, the shielding effect of a windbreak was effective, and the wind speed was between −0.2 and 0. At the windbreak transition region, the wind speed changed from negative to positive suddenly. At the cutting location, the wind speed became negative again. Due to the windbreak transition, the negative wind speed was larger towards the end of the windbreak transition, but as the distance increased along

the cutting direction, the negative values became smaller and steady in the range between −0.2 and 0, demonstrating that the shielding effect of the cutting was effective. The wind speed varied from negative to positive peak values and then changed to negative again very quickly between the flat ground and the cutting. This phenomenon was a possible cause for the yawing motion of the train and posed a safety issue for the train passing across this region.

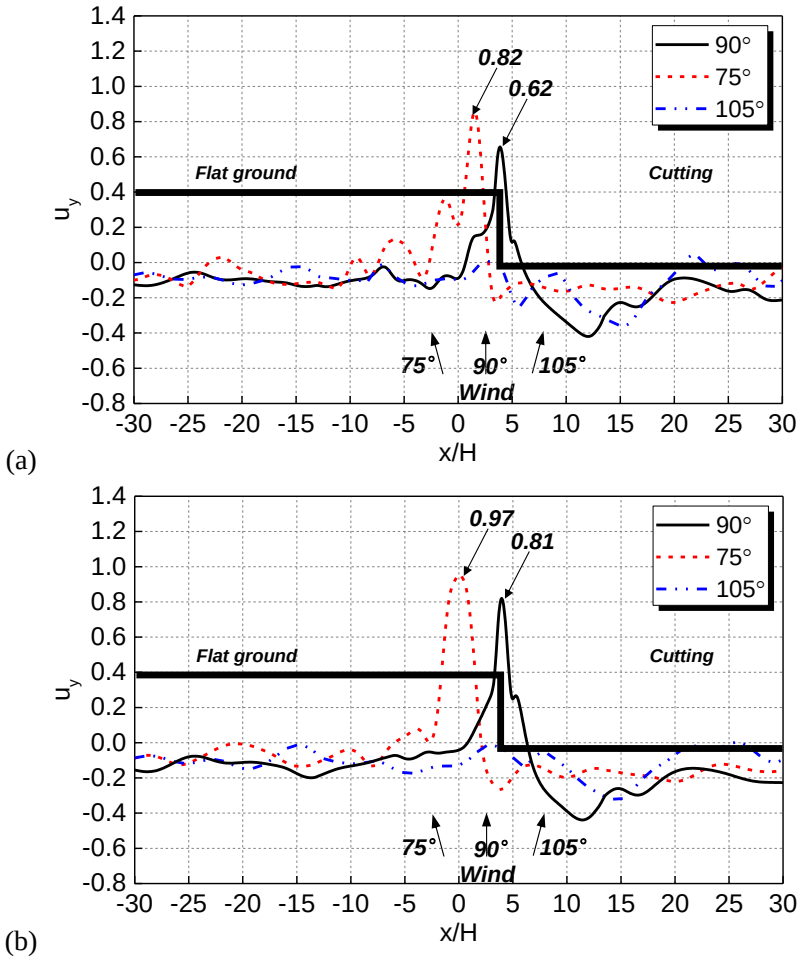

Figure 9. The wind speed along the railway: (a) RL-1 and (b) RL-2.

3.2 Flow structures of original windbreak transition

The velocity streamlines are used to describe the flow evolution and why the wind suddenly changed directions and amplitudes. At a wind angle of 90°, as shown in Figure 10(a), four vortices formed above the railway. *V*1 was generated due to compression between *V*2/*V*3 and the windbreak. The airflow ran into the railway, and *V*3 was generated. In the far flow field of the leeward side, *V*2 was generated by the strong backflow. *V*4 was generated by the backflow in the cutting. From *z*/*H* = 0.25 to 1, the structures of *V*1, *V*2, and *V*4 became larger. However, *V*3 decreased in size. Between *V*3 and *V*4, there was a strong wind speed area, as shown in the dashed box, and a mutually reinforcing effect of the sudden wind speed and vortices *V*2–*V*4 occurred. Therefore, the wind speed also became larger as the height increased. At a wind angle 75° in Figure 10(b), similar to the wind angle of 90°, four vortices formed in the windbreak transition region, but the position of the vortex changed due to the effect of the wind angle. The unperturbed freestream flow generates *V*1. *V*2 and *V*3 were generated by the backflow of the far-field on the LWS of RL-2. The airflow inside the cutting was impacted by the wind angle and tended to move in the flat ground direction, but it was blocked by *V*2 and *V*3, causing the formation of *V*4 near the opening of the

cutting. As the height increased, the core of *V*1 was closer to the windbreak. *V*2 and *V*3 moved to the LWS and away from the railway lines. *V*4 became smaller and steadier eventually. Similar to 90°, the wind speed was larger at the higher position, as shown in the dashed box, and it was the largest beside *V*2 and *V*3. However, compared to the 90° wind angle, the wind speed was high on the side of the flat ground. At a wind angle of 105° in Figure 10(c), outside the windbreak, *V*1 was generated by the corner between the windbreak and the slope. Inside the windbreak, *V*3 was generated by the connection at the windbreak. Due to the wind angle, the airflow came from the flat ground to the cutting and was subsequently blocked by the cutting, leading to *V*2 generation. The air flowed from the outside of the transition and was blocked by the LWS of the cutting wall, and thus *V*4 was generated by the backflow. As the height changed from *z/H* = 0.25 to 1, *V*1 and *V*3 changed slightly due to the limited space. In the lower position, *V*2 was invisible, and as the height increased, the core of *V*2 was more evident and moved to the LWS. Meanwhile, compared to wind angles of 90° and 75°, as shown in the dashed box, a high wind speed appeared only at *z/H* =1, and no high wind speeds appeared below the train height. This phenomenon occurred at 105° possibly due to the shielding effect of the slope and the connection of the windbreak from the flat ground to cutting. The slope raised the airflow, preventing air from flowing directly into the railway line, and it avoided strong flow within the bounds of the train height. The connecting section of the windbreak also played a certain role in restraining the wind field because it faced the wind angle direction.

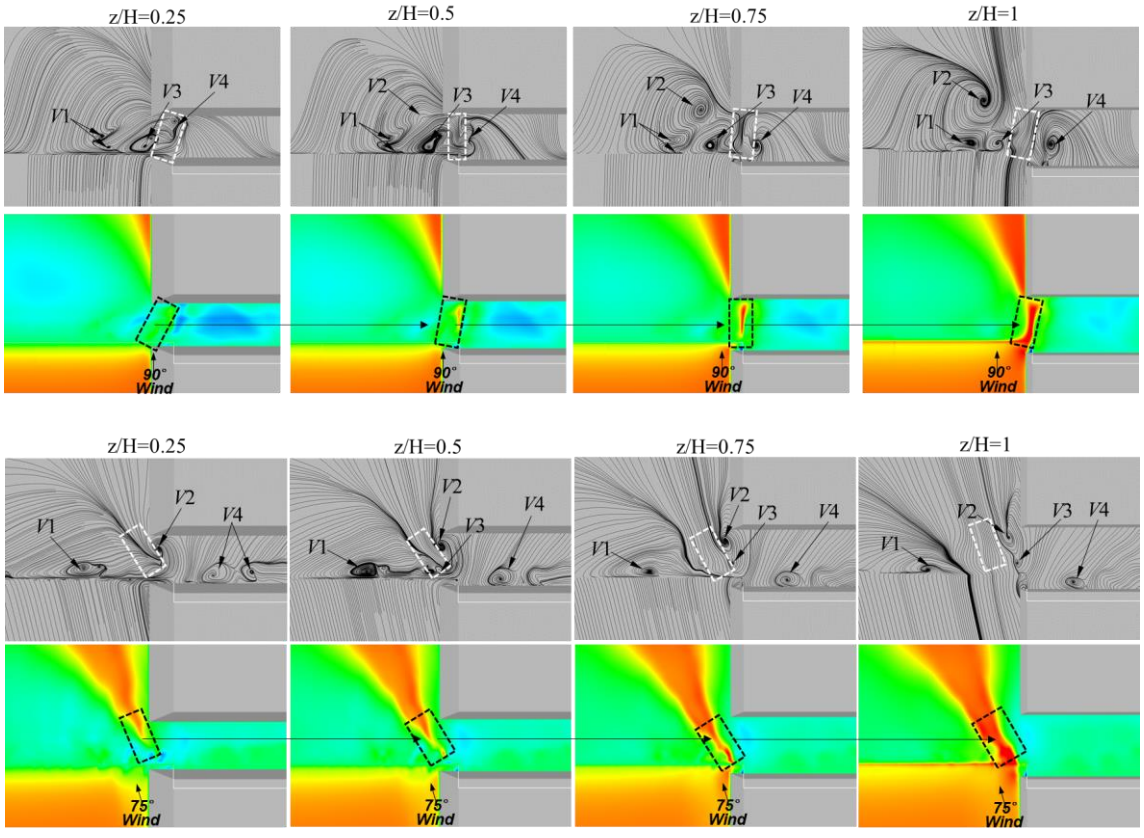

(a)

(b)

(c)

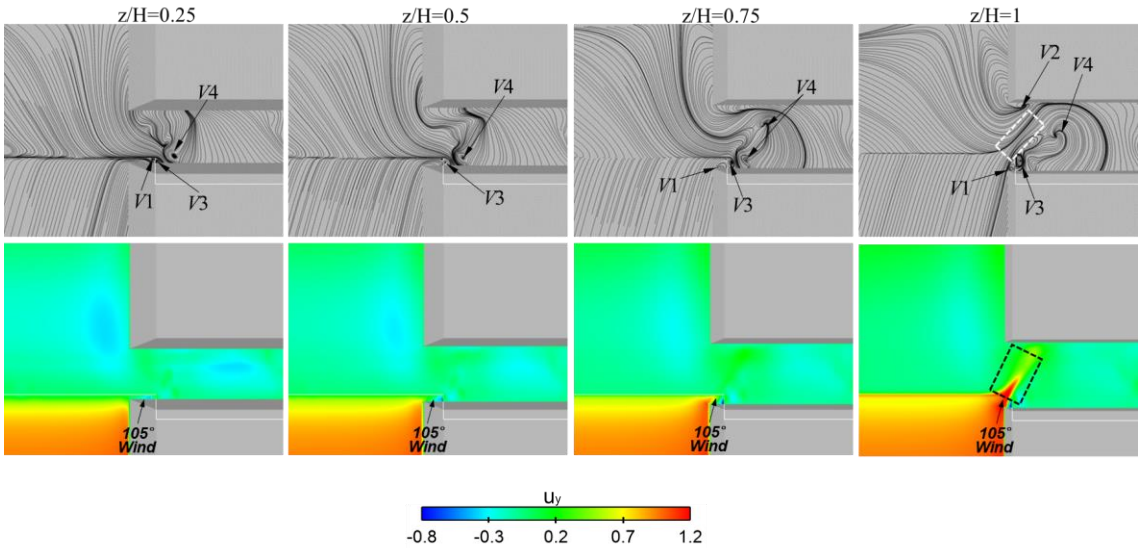

Figure 10. The streamline and speed contour at different heights for wind angles of (a) 90°, (b) 75° and (c) 105°.

Furthermore, Figure 11(a) clearly shows the source of the vortices and the strong wind speeds that occurred on the railway at the wind angles of 90°. The airflow mainly came from region A around the windbreak transition area. Due to the insufficient height of the windbreak in the slope position and the right-angle structure of the windbreak, the upstream airflow changed in speed and direction. It then rushed into the railway and led to the sudden strong wind area and generated *V*1–*V*4. At a wind angles of 75° in Figure 11(b), similar to the 90° case, region A was a region where the airflow rushed into the railway and generated *V*1–*V*3. Region B was the region of the airflow that only ran through *V*1–*V*3, and it was the source of *V*4 (as shown in Figure 10). Figure 11(c) shows the streamlines in the transition region at the wind angles of 105°, which were different from those at 90° and 75°. The airflow effect in the cutting disappeared due to the wind angle, as it entered the cutting instead of coming from the cutting. The source of *V*2–*V*4 was mainly from the left of the flat ground. After the airflow generated *V*2–*V*4, it then flowed up and left the cutting, finally moving downstream. The airflow that entered from outside the transition region was low in intensity, resulting in a lower wind speed compared to those in the 90° and 75° cases overall.

(a)

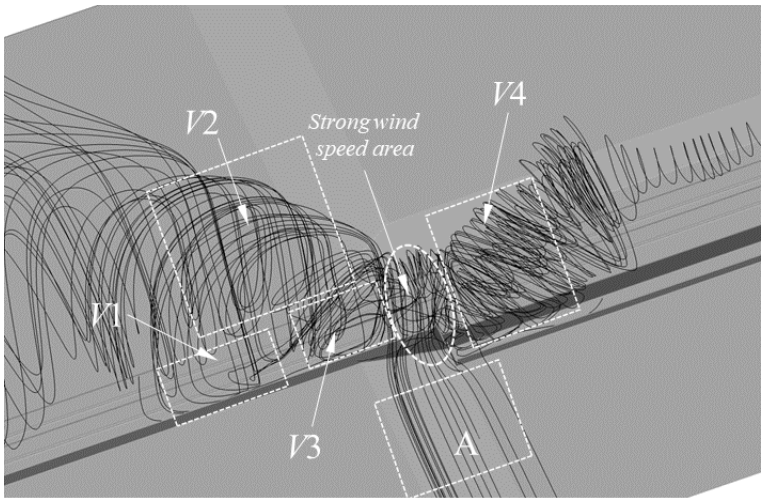

(b)

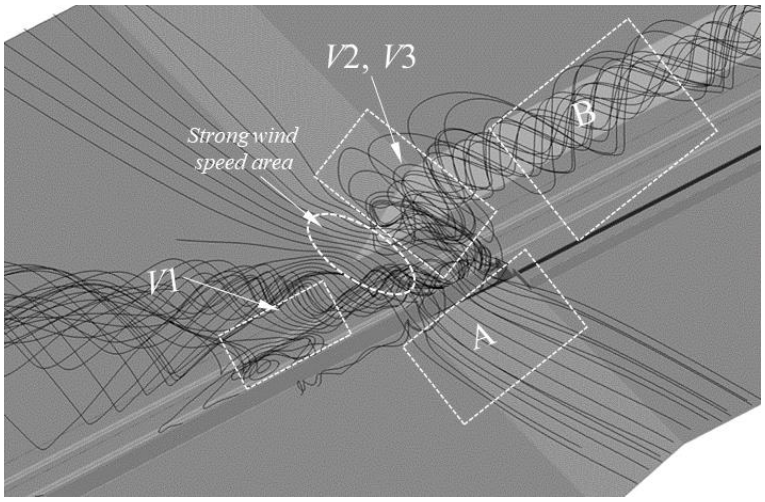

(c)

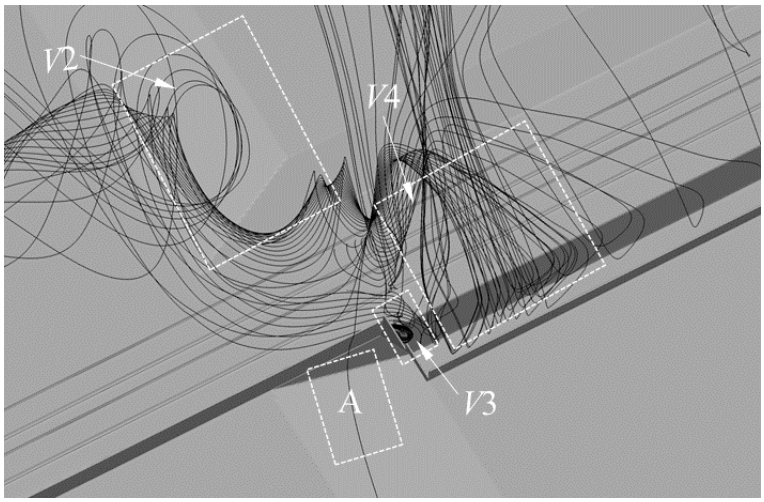

Figure 11. The space streamlines in the region of windbreak transition for wind angles of (a) 90°, (b) 75° and (c) 105°.

Finally, to show the effect of the windbreak transition on the wind speed distribution above the railway intuitively, the speed contours in the centre between RL-1 and RL-2 are shown in Figure 12. At a wind angle of 90° in Figure 12(a), below the height z/H = 1, the wind speed in the flat ground and cutting areas were all negative and small values, but there was a sudden positive wind speed value (larger than 0.75) between them that was induced by the windbreak transition. Figure 12(b) shows the speed contours at a wind angle of 75°. Due to the transition region, the left side near the flat ground, the wind speed value had a high positive value and was greater than 0.8 below z/H = 1. Figure 12(c) shows the overall speed contours at a wind angle of 105°. The transition had a minimal effect compared to the 90° and 75° cases. The sudden speed value was not larger than 0.25 along railway lines below the height z/H = 1.

(a)

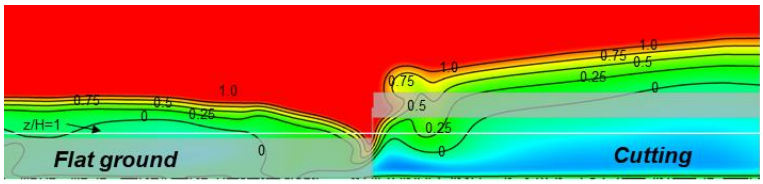

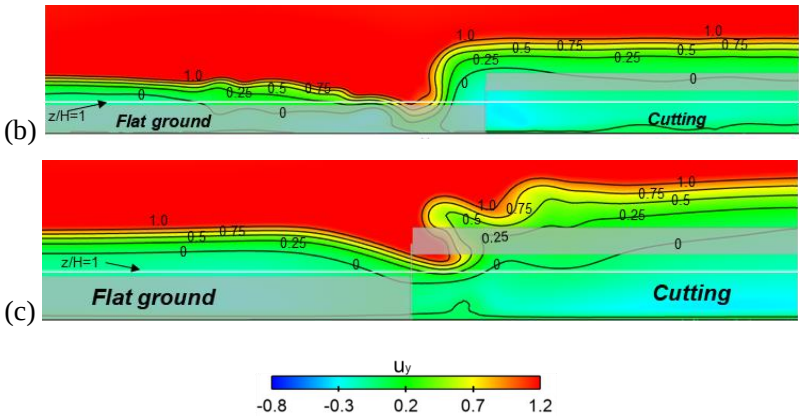

Figure 12. The speed contour in the centre between RL-1 and RL-2 for wind angles of (a) 90°, (b) 75° and (c) 105°.

4. Mitigation measures

4.1 Oblique structure (OS) transition and circular curve structure (CCS) transition

Based on the analysis in the previous sections, it was concluded that the sudden change of the flow field in the transition section was due to the height mismatch of the windbreak from the flat ground to the cutting and the interaction effect of the right-angle connection structure. Therefore, mitigation measures were proposed to ensure a reasonable transition height of the windbreak in the transition section and subsequently avoid the presence of a right-angle connection structure. On this basis, two kinds of mitigation measures were proposed: an oblique structure (OS) transition and a circular curve structure (CCS) transition, as shown in Figure 13. Figure 13(a) shows the schematic diagram of the OS transition. The concrete connection structure extended 5 m in the direction of the flat ground as the starting point of the OS transition, and the top of the cutting was used as the endpoint. The height of the OS transition was directly connected with the top of the windbreak on the flat ground and the top of the windbreak on the cutting to ensure the height of windbreak in the transition increased gradually and gently. Figure 13(b) shows a schematic diagram of the transition of the CCS. Its starting point, endpoint, and height were the same as those of the OS transition, except that the transition type was composed of two circular curves. As shown in Figure 13(b), the ends of the circular curve were tangent to points A and B on the flat ground and cutting windbreak, respectively. Point C was defined as the midpoint between the straight line AB, and point D was the midpoint between a straight line AC. DE was perpendicular to AC, making line AE perpendicular to the windbreak of the flat ground. The intersection point E was the centre of the circle, and AE was the radius of the circle. The two circular curves were tangent to point C.

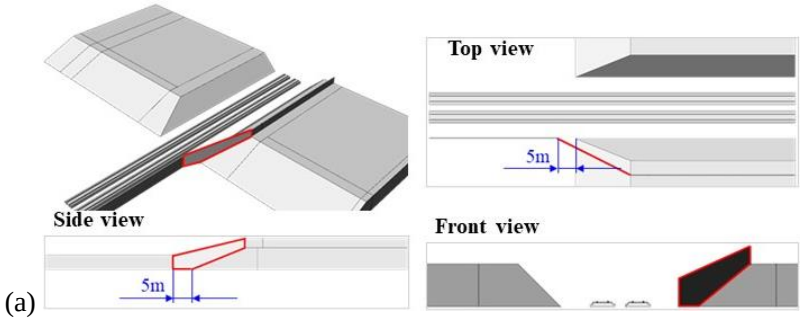

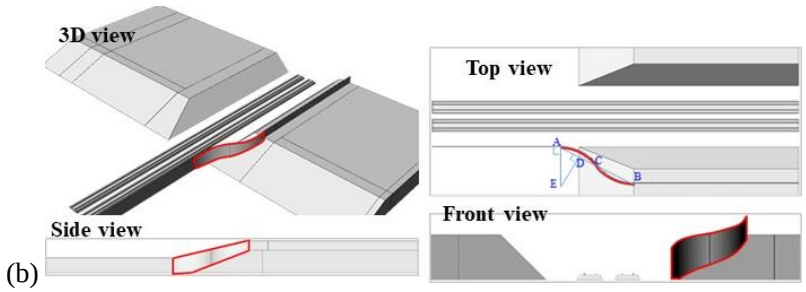

(b)

Figure 13. Mitigation measures: (a) Oblique structure and (b) Circular curve structure.

4.2 Wind speed of OS and CCS transition

Figure 14 compares the wind speeds obtained from the original, OS, and CCS transitions. Both the OS and CCS transitions reduced the peak value of the wind speed on the railway and allowed a steadier variance of the wind speed. Around the windbreak transition region (x/H= –10 to 10), for the RL-1 at a wind angle of 90°, the wind speed varied in the range of −0.3 to 0.15 for the OS transition and −0.4 to 0.1 for the CCS transition. At a wind angle of 75°, the corresponding range was −0.3 to 0. At wind angle of 105°, the range was −0.2 to 0.05. For the RL-2, the ranges were −0.35 to 0.05 for the OS transition and −0.42 to 0.05 for the CCS transition at a wind angle of 90°, −0.3 to 0 for the OS transition and −0.3 to 0.22 for the CCS transition at a wind angle of 75°, and −0.25 to 0 for the OS and CCS transitions at a wind angle 105°. Overall, the effects of the two transitions were comparable and close at different wind angles, but for convenience of construction, the OS transition is recommended.

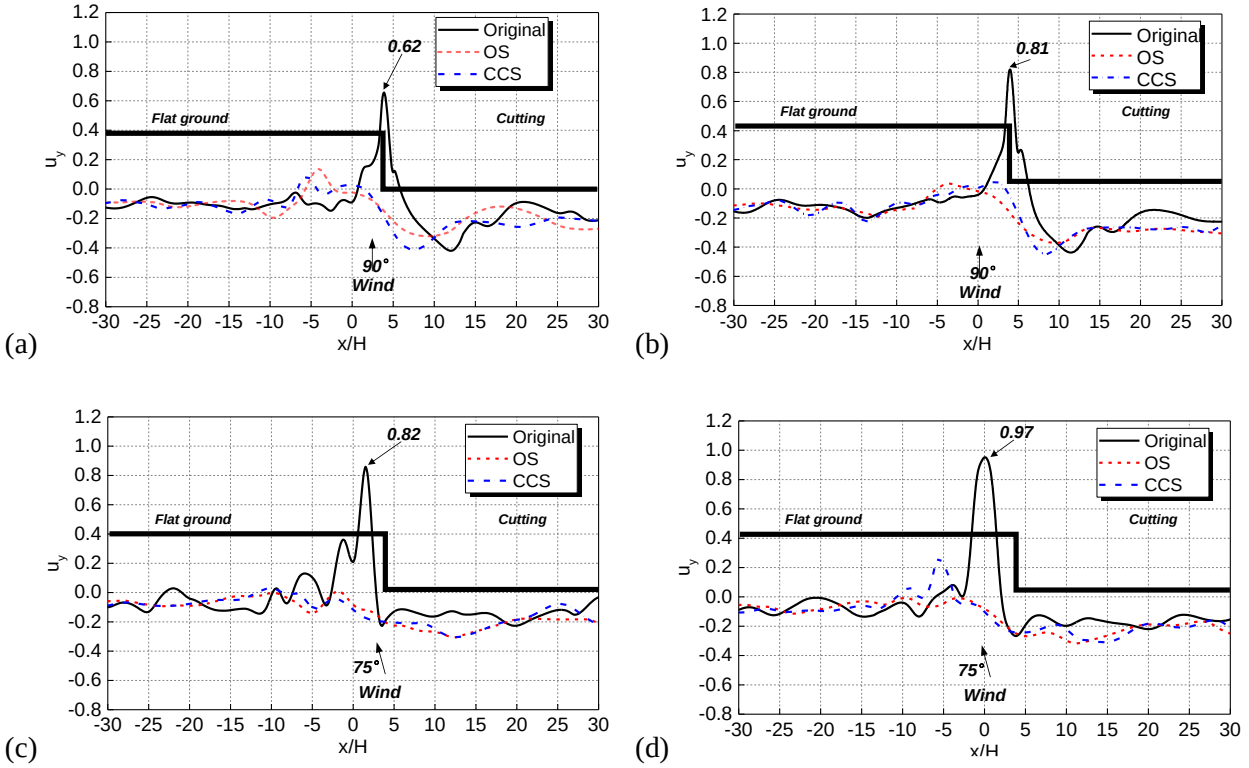

(a) (b) (c) (d)

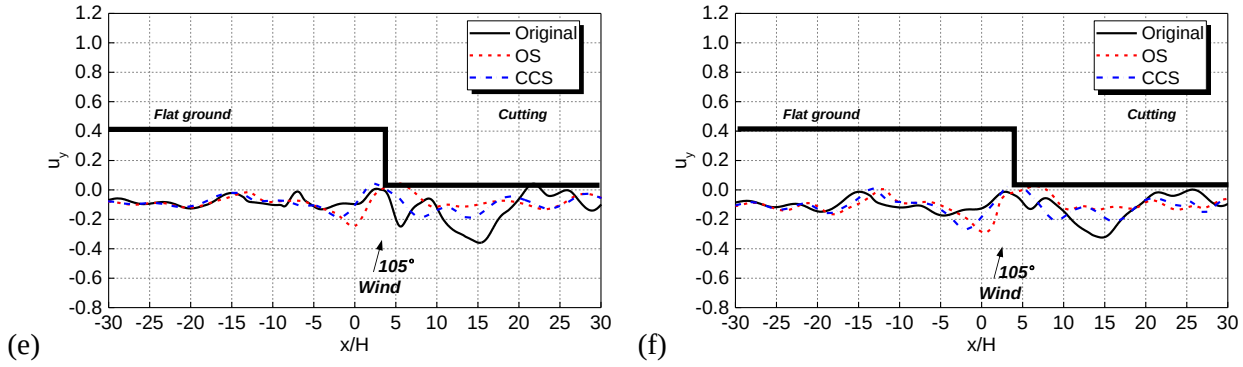

Figure 14. The wind speed along the railway: (a) RL-1 at 90°, (b) RL-2 at 90°, (c) RL-1 at 75°, (d) RL-2 at 75°, (e) RL-1 at 105° and (f) RL-2 at 105°.

4.3 Flow structures of OS and CCS transition

4.3.1 Wind angle of 90°. Based on the wind speed distribution curve, the flow structures of the OS and CCS transitions were compared. Figure 15 shows the flow structures of the OS and CCS transitions. Small vortices *V*1 and *V*2 appeared on the flat ground at low positions due to the compression effect of the windbreak, which caused the formation of vortices *V*3 & *V*4 in the transition region. However, due to the smoother connection from flat ground to the cutting, *V*3 in the CCS transition was closer to the flat ground direction. Additionally, compared to the OS transition, the outside slope of CCS changed rapidly, causing vortex generation outside the CCS transition, as shown in the white dashed box in Figure 15(b). Overall, due to the smoother transitions of both structures, the streamlines in the windbreak transition region exited in the flat ground direction. The speed contours showed that there were no sudden peak values and only small positive values occurred in the flat ground region at the starting point of the transition. Furthermore, the space streamlines in Figure 16 showed there was very little airflow travelling from the outside into the railway lines due to the improved transition. Therefore, *V*3 and *V*4 were generated only by the backflow of air that came from the cutting. As shown in Figure 17, along the railway below the height z/H = 1, smaller positive values (wind speed coefficient is less than 0.2) appeared in the flat ground direction at the starting position of the windbreak transition.

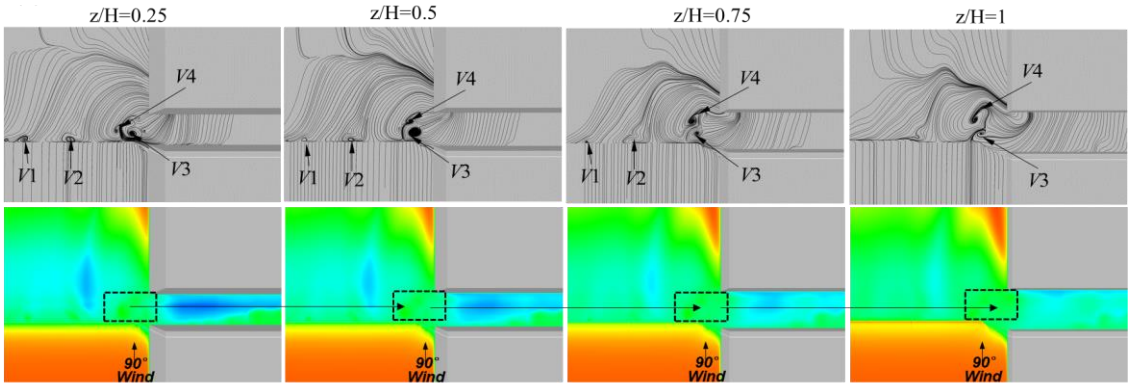

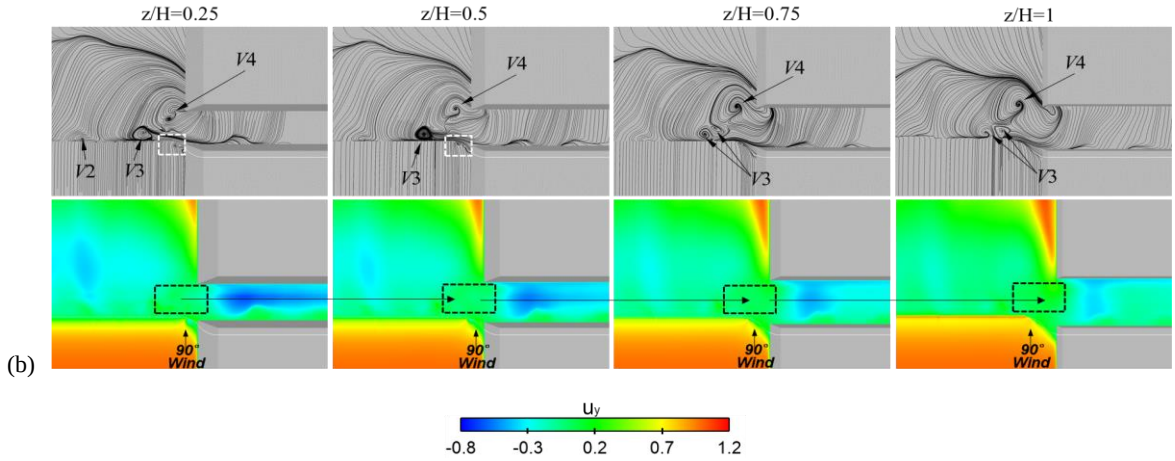

Figure 15. Streamlines and speed contours at different heights for wind angle of 90°: (a) oblique structure (OS) transition and (b) circular curve structure (CCS) transition.

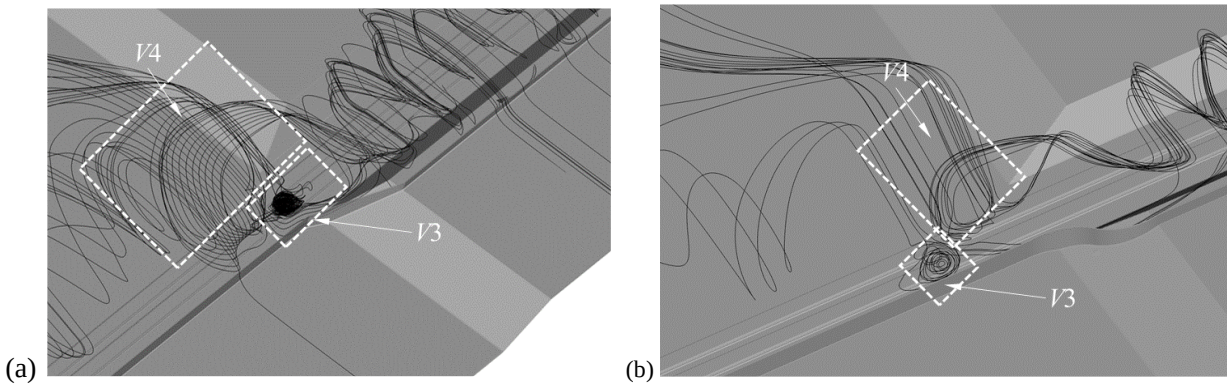

Figure 16. Streamlines for wind angle of 90°: (a) OS transition and (b) CCS transition.

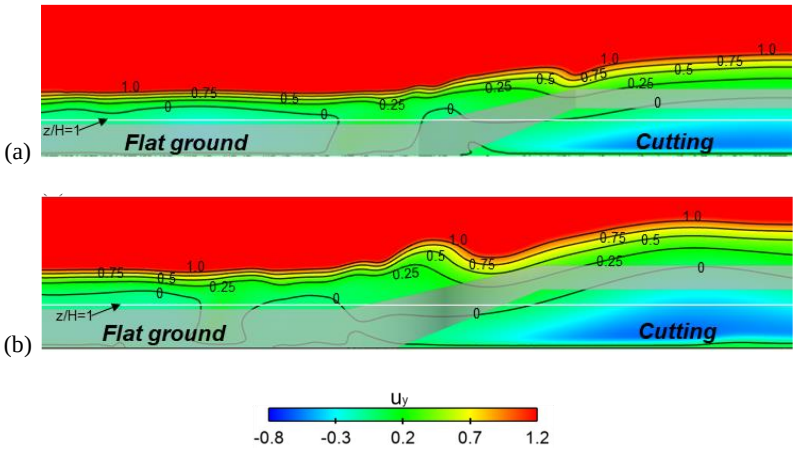

Figure 17. Speed contours in the centre between RL-1 and RL-2 for wind angle of 90°: (a) OS transition and (b) CCS transition.

4.3.2 Wind angle 75°. Figure 18 shows that on the flat ground, *V*2 (OS), *V*3 (OS), and *V*3 (CCS) formed along the railway, and the size decreased with an increase in height. For both structures, the transition form had a more significant guiding effect on the airflow caused by the wind direction, and the airflow ran along the railway in the windbreak transition region at *z*/*H* = 0.25–1 for the OS transition and at *z*/*H* = 0.25–0.75 for the CCS transition. However, as shown in the dashed box in Figure 18(b), the airflow ran through the windbreak and impacted the railway above *z*/*H* = 0.75. This was due to the discontinuous slope of the CCS, in contrast to the OS transition. This phenomenon is shown clearly in Figure 19, which demonstrated that the vortex for the

OS transition was generated by the backflow that came from the cutting, similar to the 90° case. However, for the CCS transition, the unperturbed freestream flow rushed into the railway and induced a slight strong wind area above *z/H* = 0.75.

Furthermore, as shown in Figure 20, below *z/H* = 1, there were no peak values for the OS transition, and the wind speeds were small and negative from the flat ground to the cutting. However, a large positive wind speed coefficient (0.5) was obtained for the CCS transition near the height *z/H* = 1.

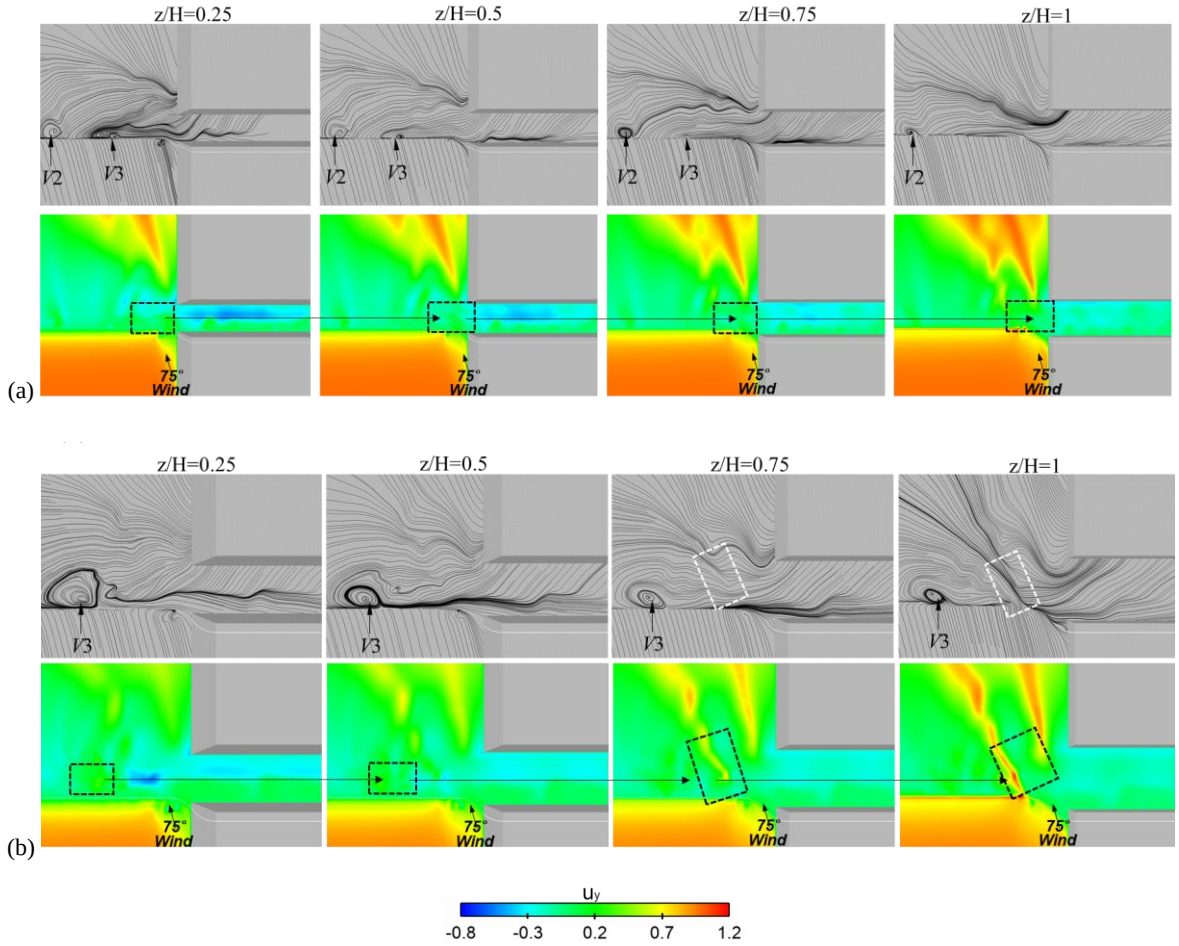

Figure 18. Streamlines and speed contours at different heights for wind angle of 75°: (a) OS transition and (b) CCS transition.

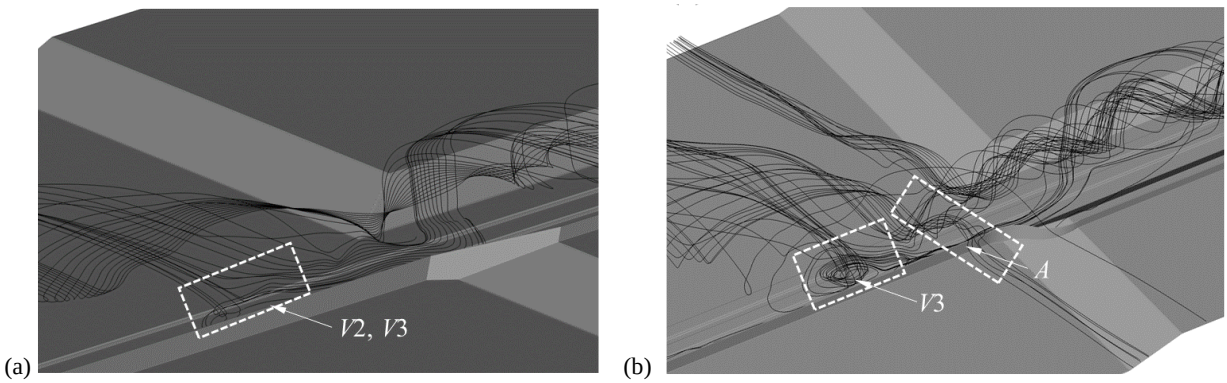

Figure 19. Streamlines for wind angle 75°: (a) OS transition and (b) CCS transition.

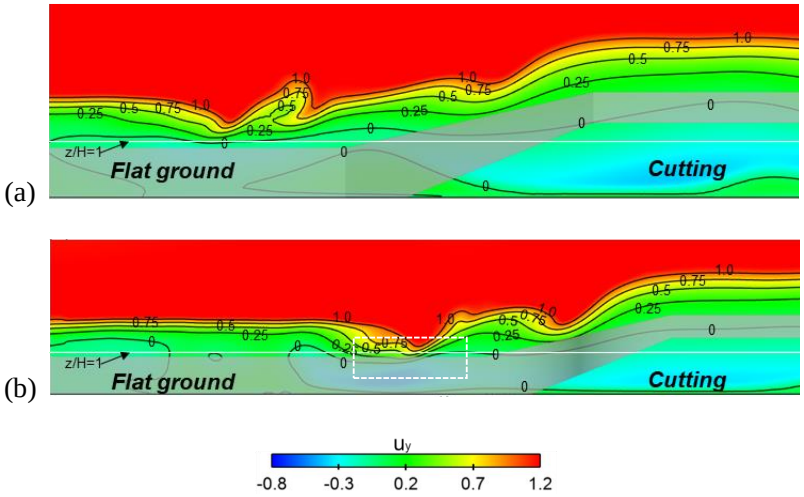

Figure 20. Speed contours in the centre between RL-1 and RL-2 for wind angle of 75°: (a) OS transition and (b) CCS transition.

4.3.3 Wind angle of 105°. At a wind angle of 105°, the airflow inside the railway came from the flat ground for both transitions. Figure 21 shows that *V*3 was generated at the starting position of the transition, and *V*4 was generated in the cutting near the end of the transition. Additionally, *V*1 and *V*2 were generated by the backflow that was blocked by *V*4 in the cutting. As the height increased, *V*4 became larger and occupied the entire width of the cutting at height *z*/*H* = 1. Both transitions did not exhibit any sudden positive wind speed values along the railway. As shown in Figure 22, the airflow that generated vortices in the transition region arose from the flat ground, and there was no airflow from outside the windbreak, indicating that both the OS and CCS transitions yielded better performances at a wind angle of 105°. As shown in Figure 23, the positive wind speed values in the end positions of the OS and CCS transitions were not larger than 0.2.

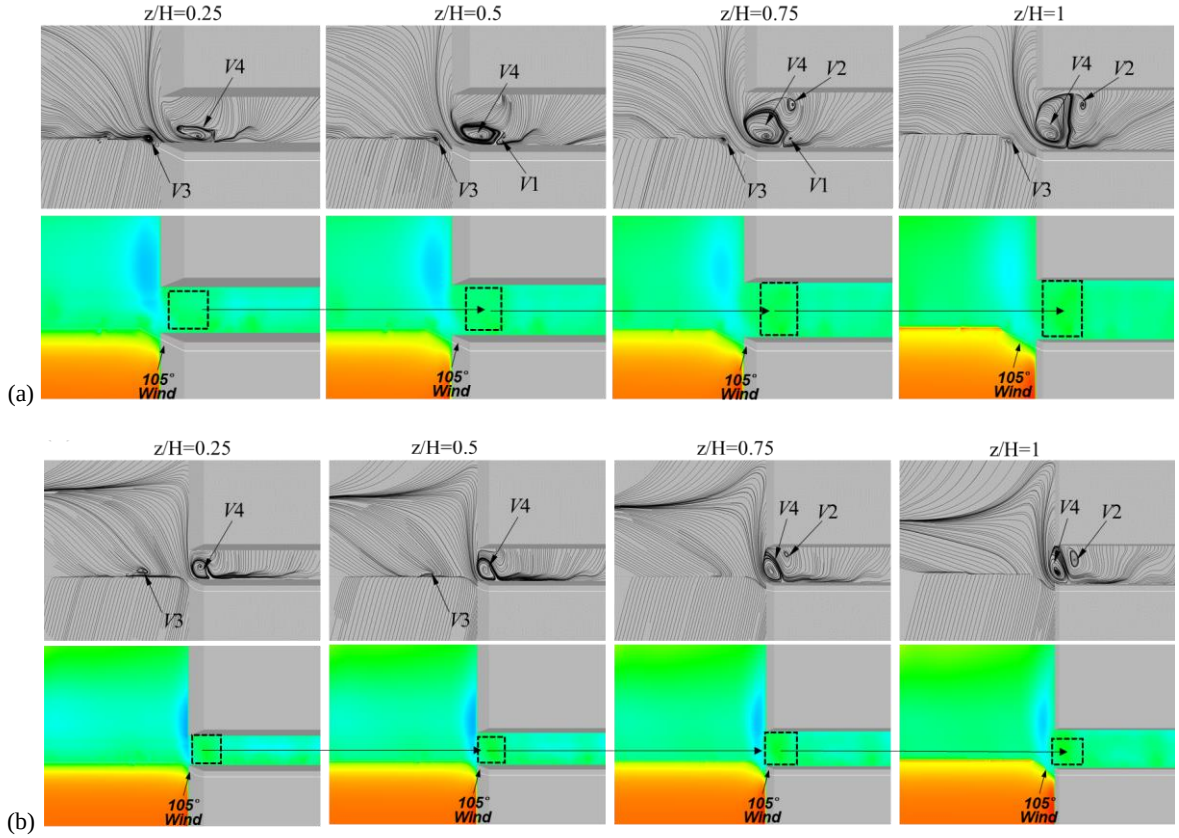

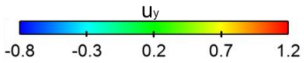

Figure 21. Streamlines and speed contours at different heights for wind angle of 105°: (a) OS transition and (b) CCS transition.

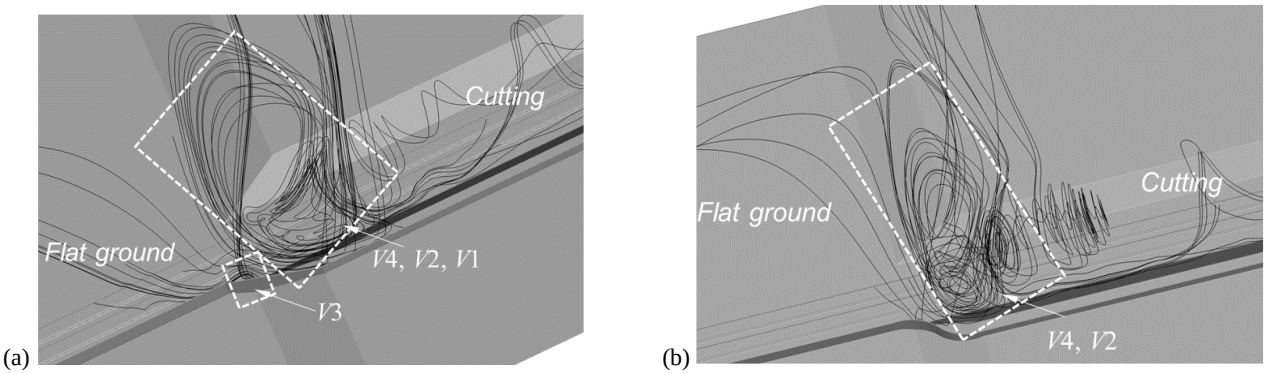

Figure 22. Streamlines for wind angle of 105°: (a) OS transition and (b) CCS transition.

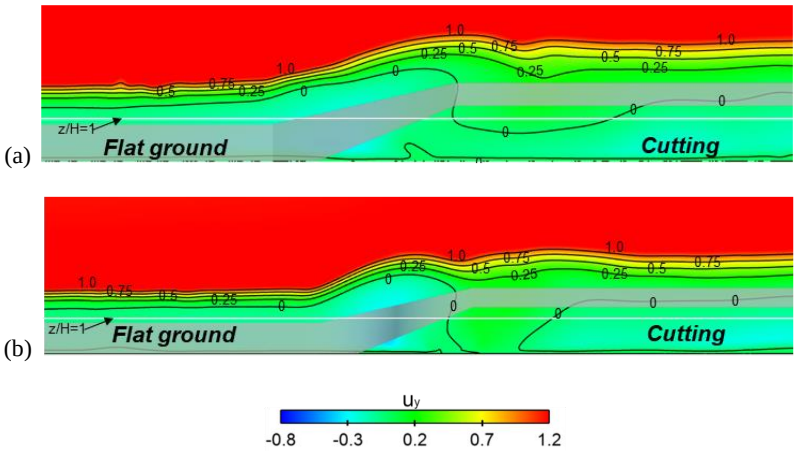

Figure 23. Speed contours in the centre between RL-1 and RL-2 for wind angle of 105°: (a) OS transition and (b) CCS transition.

Based on the results in Sections 3 and 4, under the effect of the terrain and different wind angles, the windbreak transition has a large impact on the wind speed distribution and flow structures of railway lines. In the present work, it was found that the effect of a wind angle of 75° was the largest, due to the wind angle being aligned with the slope, followed by 90°, and finally 105°. This was possibly due to the slope and the windbreak connection from flat ground to the cutting providing an extra shielding effect. At wind angles of 90° and 75°, the wind speeds on the railway lines were larger than 0.6, and the sudden strong wind speed areas were all induced by the windbreak transition. However, due to the effect of the wind angle, the position of the strong wind speed was different: at a wind angle 90°, it was at x/H = 3 to 6, and at wind angle 75°, it was at x/H= −2.5 to 2.5.

Both the OS and CCS transitions were effective in reducing the rapid wind speed change of the railway. However, the CCS transition was worse than the OS transition at a wind angle of 75°. Furthermore, since the OS transition is easy to construct, it was recommended to be used in practice.

5. Conclusions

In this paper, the flow field deterioration mechanism induced by the inappropriate form of a windbreak transition at three wind angles was examined, and effective mitigation and improvement measures, oblique structure (OS) and circular curve structure (CCS) transition, were proposed and evaluated.

(1) For the original windbreak transition, at a height range higher than half of the train height, the sudden peak values of the dimensionless wind speed in the windbreak transition area were in the range of 0.62 – 0.97 at different wind angles. Different vortices formed around the windbreak transition region, resulting in strong wind speed areas. This area occurred near the cutting position for a wind angle of 90°, and it occurred near the flat ground for a wind angle of 75°.

(2) The velocity streamlines were used to find the sources of the vortices that formed along the railway lines, demonstrating why a sudden, strong, positive wind speed area formed. First, the height mismatch in the transition region resulted in weak protection from the windbreak. Second, the right-angle structure of the windbreak transition resulted in a sudden change in the wind speed and flow direction.

(3) The OS and CCS transition reduced the positive peak wind speed in the original transition region. The peak value of dimensionless wind velocity was all less than 0.2 for OS and CCS. However, the OS transition was better in terms of overall protection and convenience of construction, which make it a better candidate to adopt in practice.

References

ANSYS, 2013. ANSYS Fluent Theory Guide. ANSYS, Inc., Canonsburg, PA.

Baker, C., Cheli, F., Orellano, A., Paradot, N., Proppe, C. and Rocchi, D. (2009), "Cross-wind effects on road and rail vehicles", *Vehicle System Dynamics*, Vol. 47 No. 8, pp. 983-1022.

Chen, Z., Liu, T., Jiang, Z., Guo, Z. and Zhang, J. (2018), "Comparative analysis of the effect of different nose lengths on train aerodynamic performance under crosswind", *Journal of Fluids and Structures*, Vol. 78, pp. 69-85.

Chen, Z., Liu, T., Li, M., Yu, M., Lu, Z. and Liu, D. (2019a), "Dynamic response of railway vehicles under unsteady aerodynamic forces caused by local landforms", *Wind and Structures*, Vol. 29 No. 3, pp. 149-161.

Chen, Z., Liu, T., Li, W., Guo, Z. and Xia, Y. (2021), "Aerodynamic performance and dynamic behaviors of a train passing through an elongated hillock region beside a windbreak under crosswinds and corresponding flow mitigation measures", *Journal of Wind Engineering and Industrial Aerodynamics*, Vol. 208, p. 104434.

Chen, Z., Liu, T., Yan, C., Yu, M., Guo, Z. and Wang, T. (2019b), "Numerical simulation and comparison of the slipstreams of trains with different nose lengths under crosswind", *Journal of Wind Engineering and Industrial Aerodynamics*, Vol. 190, pp. 256-272.

Chen, Z., Liu, T., Zhou, X. and Niu, J. (2017), "Impact of ambient wind on aerodynamic performance when two trains intersect inside a tunnel", *Journal of Wind Engineering and Industrial Aerodynamics*, Vol. 169, pp. 139-155.

Chen, Z. and Ni, Y. (2022), "Sudden flow induced by mountain ridges beside windbreaks in a railway and its mitigation measures", *Transportation Safety and Environment*, Vol. 4 No. 1, p. tdac004.

Chen, Z., Rui, E., Liu, T., Ni, Y., Huo, X., Xia, Y., Li, W., Guo, Z. and Zhou, L. (2022), "Unsteady Aerodynamic Characteristics of a High-Speed Train Induced by the Sudden Change of Windbreak Wall Structure: A Case Study of the Xinjiang Railway", Vol. 12 No. 14, p. 7217.

Cui, T., Zhang, W. and Sun, B. (2014), "Investigation of train safety domain in cross wind in respect of attitude change", *Journal of Wind Engineering and Industrial Aerodynamics*, Vol. 130, pp. 75-87.

Deng, E., Yang, W., Lei, M., Zhu, Z. and Zhang, P. (2019), "Aerodynamic loads and traffic safety of high-speed trains when passing through two windproof facilities under crosswind: A comparative study", *Engineering Structures*, Vol. 188, pp. 320-339.

Diedrichs, B., Sima, M., Orellano, A. and Tengstrand, H. (2007), "Crosswind stability of a high-speed train on a high embankment", *Proceedings of the Institution of Mechanical Engineers, Part F: Journal of Rail and Rapid Transit*, Vol. 221 No. 2, pp. 205-225.

Flynn, D., Hemida, H., Soper, D. and Baker, C. (2014), "Detached-eddy simulation of the slipstream of an operational freight train", *Journal of Wind Engineering and Industrial Aerodynamics*, Vol. 132, pp. 1-12.

Gao, H., Liu, T., Gu, H., Jiang, Z., Huo, X., Xia, Y. and Chen, Z. (2021), "Full-scale tests of unsteady aerodynamic loads and pressure distribution on fast trains in crosswinds", *Measurement*, Vol. 186, p. 110152.

Gu, H., Liu, T., Jiang, Z. and Guo, Z. (2020), "Research on the wind-sheltering performance of different forms of corrugated wind barriers on railway bridges", *Journal of Wind Engineering and Industrial Aerodynamics*, Vol. 201, p. 104166.

Guo, Z., Liu, T., Chen, Z., Liu, Z., Monzer, A. and Sheridan, J. (2020), "Study of the flow around railway embankment of different heights with and without trains", *Journal of Wind Engineering and Industrial Aerodynamics*, Vol. 202, p. 104203.

Guo, Z., Liu, T., Yu, M., Chen, Z., Li, W., Huo, X. and Liu, H. (2019), "Numerical study for the aerodynamic performance of double unit train under crosswind", *Journal of Wind Engineering and Industrial Aerodynamics*, Vol. 191, pp. 203-214.

He, X., Zhou, L., Chen, Z., Jing, H., Zou, Y. and Wu, T. (2019), "Effect of wind barriers on the flow field and aerodynamic forces of a train–bridge system", *Proceedings of the Institution of Mechanical Engineers, Part F: Journal of Rail and Rapid Transit*, Vol. 233 No. 3, pp. 283-297.

He, X., Zuo, T., Zou, Y., Yan, L. and Tang, L. (2020), "Experimental study on aerodynamic characteristics of a high-speed train on viaducts in turbulent crosswinds", *Journal of Central South University*, Vol. 27 No. 8, pp. 2465-2478.

Hemida, H. and Krajnović, S. (2009), "Exploring flow structures around a simplified ICE2 train subjected to a 30 side wind using LES", *Engineering Applications of Computational Fluid Mechanics*, Vol. 3 No. 1, pp. 28-41.

Hu, P., Li, Y., Huang, G., Kang, R. and Liao, H. (2015), "The appropriate shape of the boundary transition section for a mountain-gorge terrain model in a wind tunnel test", *Wind and Structures*, Vol. 20 No. 1, pp. 15-36.

Huang, G., Cheng, X., Peng, L. and Li, M. (2018), "Aerodynamic shape of transition curve for truncated mountainous terrain model in wind field simulation", *Journal of Wind Engineering and Industrial Aerodynamics*, Vol. 178, pp. 80-90.

Huang, S., Hemida, H. and Yang, M. (2016), "Numerical calculation of the slipstream generated by a CRH2 high-speed train", *Proceedings of the Institution of Mechanical Engineers, Part F: Journal of Rail and Rapid Transit*, Vol. 230 No. 1, pp. 103-116.

Kondo, K., Tsuchiya, M. and Sanada, S. (2002), "Evaluation of effect of micro-topography on design wind velocity", *Journal of Wind Engineering and Industrial Aerodynamics*, Vol. 90 No. 12, pp. 1707-1718.

Krajnović, S., Ringqvist, P., Nakade, K. and Basara, B. (2012), "Large eddy simulation of the flow around a simplified train moving through a crosswind flow", *Journal of Wind Engineering and Industrial Aerodynamics*, Vol. 110, pp. 86-99.

Li, T., Zhang, J. and Zhang, W. (2013), "A numerical approach to the interaction between airflow and a high-speed train subjected to crosswind", *Journal of Zhejiang University-SCIENCE A*, Vol. 14 No. 7, pp. 482-493.

Li, W., Liu, T., Martinez-Vazquez, P., Guo, Z., Huo, X., Xia, Y. and Chen, Z. (2022), "Effects of embankment layouts on train aerodynamics in a wind tunnel configuration", *Journal of Wind Engineering and Industrial Aerodynamics*, Vol. 220, p. 104830.

Li, Y., Zhang, J., Zhang, M., Wang, Z. and Guo, J. (2019), "Aerodynamic effects of viaduct-cutting connection section on high-speed railway by wind tunnel tests", *Journal of Aerospace Engineering*, Vol. 32 No. 5, p. 05019002.

Liu, C., Bu, W., Xu, D., Lei, Y. and Li, X. (2017), "Application of hybrid RANS/LES turbulence models in rotor-stator fluid machinery: a comparative study", *International Journal of Numerical Methods for Heat & Fluid Flow*, Vol. 27 No. 12, pp. 2717-2743.

Liu, D., Wang, Q., Zhong, M., Lu, Z., Wang, J., Wang, T. and Lv, S. (2019), "Effect of wind speed variation on the dynamics of a high-speed train", *Vehicle System Dynamics*, Vol. 57 No. 2, pp. 247-268.

Liu, T., Chen, Z., Zhou, X. and Zhang, J. (2018), "A CFD analysis of the aerodynamics of a high-speed train passing through a windbreak transition under crosswind", *Engineering Applications of Computational Fluid Mechanics*, Vol. 12 No. 1, pp. 137-151.

Liu, T., Wang, L., Chen, Z., Gao, H., Li, W., Guo, Z., Xia, Y., Huo, X. and Wang, Y. (2022), "Study on the pressure pipe length in train aerodynamic tests and its applications in crosswinds", *Journal of Wind Engineering and Industrial Aerodynamics*, Vol. 220, p. 104880.

Niu, J., Zhang, Y., Li, R., Chen, Z., Yao, H. and Wang, Y. (2022), "Aerodynamic simulation of effects of one- and two-side windbreak walls on a moving train running on a double track railway line subjected to strong crosswind", *Journal of Wind Engineering and Industrial Aerodynamics*, Vol. 221, p. 104912.

Shao, X., Wan, J., Chen, D. and Xiong, H. (2011), "Aerodynamic modeling and stability analysis of a high-speed train under strong rain and crosswind conditions", *Journal of Zhejiang University-SCIENCE A*, Vol. 12 No. 12, pp. 964-970.

Shur, M.L., Spalart, P.R., Strelets, M.K. and Travin, A.K. (2008), "A hybrid RANS-LES approach with delayed-DES and wall-modelled LES capabilities", *International Journal of Heat and Fluid Flow*, Vol. 29 No. 6, pp. 1638-1649.

Spalart, P.R., Deck, S., Shur, M.L., Squires, K.D., Strelets, M.K. and Travin, A. (2006), "A new version of detached-eddy simulation, resistant to ambiguous grid densities", *Theoretical and Computational Fluid Dynamics*, Vol. 20 No. 3, pp. 181-195.

Sun, Z., Dai, H., Gao, H., Li, T. and Song, C. (2019), "Dynamic performance of high-speed train passing windbreak breach under unsteady crosswind", *Vehicle System Dynamics*, Vol. 57 No. 3, pp. 408-424.

Tahani, M., Masdari, M., Eivazi, H. and Tatar, M. (2017), "Assessment of turbulence models for transonic oscillating airfoil", *International Journal of Numerical Methods for Heat & Fluid Flow*, Vol. 27 No. 11, pp. 2603-2628.

TFI, 2015. Turbulent Flow Instrumentation - Cobra Probe - Getting Started Guide. Turbulent Flow Instrumentation Pty Ltd, Victoria, Australia.

Tian, H. (2010), "Research progress in railway safety under strong wind condition in China", *Journal of Central South University (Science and Technology)*, Vol. 41 No. 6, pp. 2435-2443. (in Chinese)

Tian, H. (2019), "Review of research on high-speed railway aerodynamics in China", *Transportation Safety and Environment*, Vol. 1 No. 1, pp. 1-21.

Tschepe, J., Nayeri, C.N. and Paschereit, C.O. (2021), "On the influence of Reynolds number and ground conditions on the scaling of the aerodynamic drag of trains", *Journal of Wind Engineering and Industrial Aerodynamics*, Vol. 213, p. 104594.

Van Doormaal, J.P. and Raithby, G.D. (1984), "Enhancements of the SIMPLE method for predicting incompressible fluid flows", *Numerical Heat Transfer*, Vol. 7 No. 2, pp. 147-163.

Wang, J., Minelli, G., Dong, T., Chen, G. and Krajnović, S. (2019), "The effect of bogie fairings on the slipstream and wake flow of a high-speed train. An IDDES study", *Journal of Wind Engineering and Industrial Aerodynamics*, Vol. 191, pp. 183-202.

Wang, L., Li, L. and Fu, S. (2017), "A comparative study of DES type methods for mild flow separation prediction on a NACA0015 airfoil", *International Journal of Numerical Methods for Heat & Fluid Flow*, Vol. 27 No. 11, pp. 2528-2543.

Wu, X., Zou, X., Zhang, C., Wang, R., Zhao, J. and Zhang, J. (2013), "The effect of wind barriers on airflow in a wind tunnel", *Journal of Arid Environments*, Vol. 97, pp. 73-83.

Xiang, H., Li, Y., Wang, B. and Liao, H. (2015), "Numerical simulation of the protective effect of railway wind barriers under crosswinds", *International Journal of Rail Transportation*, Vol. 3 No. 3, pp. 151-163.

Xu, J., Chen, Z. and Liu, T., 2019. Experimental and numerical research on the safety of an EMU running on a normal-speed railway line under strong wind, IOP Conference Series: Materials Science and Engineering. IOP Publishing, p. 044049.

Ye, K. and Li, R.X. (2013), "Aerodynamic Characteristics Analysis of High-Speed Train on Cutting under Crosswinds", *Applied Mechanics and Materials*, Vol. 300-301, p. 62.

Zhang, J., Gao, G. and Liu, T. (2014), "Effect of Cutting Slope Angle on Aerodynamic Performance of High-Speed Trains", *14th COTA International Conference of Transportation Professionals*, pp. 199-210.